Comparative study of space-charge effects in polymer light emitting diodes by means of reflection electro-optic and electroabsorption techniques

L. Dominici and F. Michelotti
Istituto Nazionale di Fisica della Materia-Unità dell'Università di Roma "La Sapienza," Dipartimento di Energetica, Via Antonio Scarpa, 16 I-00161 Roma, Italy

S. Whitelegg, A. Campbell, and D. D. C. Bradley
Imperial College, Blackett Laboratory, London, United Kingdom

(Received 21 July 2003; revised manuscript received 10 November 2003; published 10 February 2004)

We used two nonlinear optical techniques, single wavelength ellipsometry and electroabsorption spectroscopy, to study the creation of space charge distributions in an Al/polymer/ITO organic light emitting diode. The polymer is OXA1-PPV, a derivative of poly(*p*-phenylene-vinylene) in which oxidiazole groups are grafted as side chains to improve electroluminescence efficiency. Both the techniques are sensitive to the spatial profile of electric field via the nonlinear effect in the bulk of the polymer. Results indicate the creation of an asymmetric charge distribution with depletion region close to the ITO electrode. The comparison between ellipsometry and electroabsorption measurements is an original feature of this work. Such an integrated analysis shows as a further result that the mostly used electroabsorption setup, working with wavelengths in the spectral region of maximum absorption, modifies the spatial charge distribution optically reactivating trapped carriers.

DOI: 10.1103/PhysRevB.69.054201 PACS number(s): 72.20.Jv

I. INTRODUCTION

Organic semiconductors represent a modern class of materials for optoelectronics applications such as lighting panels, thin film transistor, solar cells, laser microcavities, and large-area flat-panel displays. At the moment, most of studied devices among these are organic and polymer light emitting diodes (OLED and PLED), representing the functional units to manufacture organic matrix displays.[1] Different materials and configurations have been proposed and studied, so that first commercial lighting displays are made possible. Anyway, lifetime and stability are limited, due to the insufficient comprehension of mechanisms related to space charge formation and device degradation.[2,3]

Conventional techniques, like static and transient I/V measurements, photoluminescence $P_{\mathrm{PL}}(\lambda)$ and electroluminescence $P_{\mathrm{EL}}(\lambda)$, impedance spectroscopy and differential capacity are indispensable and currently used for the PLED characterization. Besides these, nonlinear optical techniques represent a powerful tool to have a direct insight of material specific parameters, like nonlinear dielectric susceptibilities $\chi^{(2)}$, $\chi^{(3)}$, and of internal electric field distribution.[4–8]

We used two independent experimental configurations belonging to such family of techniques, respectively, single wavelength electro-optic ellipsometry (EO) and electroabsorption spectroscopy (EA), for probing charge distributions in poly(*p*-phenylene-vinylene) (PPV) single layer PLED. The investigations follow a previous work,[7] in which we studied devices of the same kind with thicker active layer only by means of the ellipsometric setup. The integrated analysis based upon both techniques is an original feature of the actual work. It requires an accurate theoretical and experimental study, which leads to putting into evidence the differences between the two and to relevant results about the features of space-charge distributions. In the following we will show the principles common to both EO and EA.

II. SAMPLE PREPARATION

The active layer of the studied PLED is a PPV derivative, with oxadiazole groups linked as side chains to the PPV backbone (OXA1-PPV) to improve electroluminescence efficiency (see the inset in Fig. 1). The OXA1-PPV was dissolved in 1,1,2-tetrachloroethane and spun on a glass substrates previously coated with an ITO transparent anode. An Al cathode was sputtered on the top surface, after protecting the contact points with an insulating PMMA intermediate layer, to prevent short circuits. Sample preparation is described more in detail elsewhere.[9] The thickness of the OXA1-PPV active layer is 210($\pm$10) nm, smaller than that of samples used in the precedent reported measurements (285 nm).

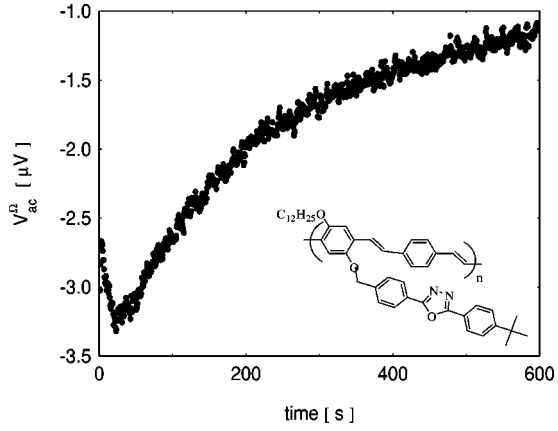

FIG. 1. Time dependence of the EO signal detected in one of the two bias point (Ψ^A) after that V_s is switched from $+7$ to -7 V.

III. PRINCIPLES OF THE TECHNIQUES

Both the setups make use of standard PLED devices for the measurements, with a typical structure of stacked layers deposited on glass substrates, as described earlier. Fundamental to both techniques used is the application of a modulated voltage of the form $V(t)=V_s+V_m\cos(\Omega t)$ between the diode terminals, giving rise to an internal electric field $E(z,t)=E_s(z)+E_m(z)\cos(\Omega t)$. A light beam at frequency $\omega \gg \Omega$, impinging on the sample from the substrate side, is reflected by the multilayer structure and modulated both at Ω and 2Ω through the quadratic electro-optic response $\chi^{(3)}$, with power amplitude that is proportional to the spatial overlap integrals of $E_s(z)$ and $E_m(z)$ in the active layer:[10]

$$\Delta P^{(\Omega)} \propto \int_0^h E_s(z)E_m(z)dz=\Gamma_1^{(\Omega)}, \tag{1}$$

$$\Delta P^{(2\Omega)} \propto \int_0^h [E_m(z)]^2 dz=\Gamma_2^{(2\Omega)}. \tag{2}$$

The sketches of the two experimental setups have been described in previous works.[4,7,8,11] Since it is possible to consider the theory of EA as a particular case of the more complex EO, we will show the equations describing them in the frame of a unified theory.

The main differences between the EA and the EO consist in the use of unpolarized and incoherent light from a lamp with monochromator, instead of an elliptically polarized laser beam ($\lambda=0.6328\ \mu$m in our case). This makes that EA is quite simple to handle experimentally and theoretically, and makes possible to change the wavelength of the measurement beam. On the other side EO allows one to obtain higher sensitivity, as will be clear in the following.

In the case of EO, the average power detected by the photodiode can be written as

$$P_{\rm dc}(\Psi_c)=\tfrac{1}{4}P_0|r_s|^2[1+(\tan\Phi)^2-2\tan\Phi\cos(\Psi_{ps}+\Psi_c)], \tag{3}$$

where P_0 is the input beam power, the angles Φ and Ψ_{ps} are defined by the relation $r_p/r_s=\tan(\Phi)e^{j\Psi_{ps}}$ and r_p and r_s are the Fresnel reflection coefficients for the *p* and *s* polarization, while the phase differences Ψ_c and Ψ_{ps} are due to the liquid-crystal retarder and to the active layer.

Upon application of the voltage $V(t)=V_s+V_m\cos(\Omega t)$, the intensity of the reflected beam is modulated both at Ω and 2Ω, due either to a phase or an amplitude modulation of the *p* and *s* components. In a general approach, the power modulation at frequency $q\Omega$ ($q=1,2$) can be obtained by differentiating the Eq. (3) with respect to the field-dependent quantities:

$$\begin{aligned}P_{\rm ac}^{(q\Omega)}(\Psi_c)&=\delta^{(q\Omega)}P_{\rm dc}\\&=\frac{1}{4}P_0|r_s|^2\Big\{[1+(\tan\Phi)^2-2\tan\Phi\cos\Psi]\\&\times\frac{\delta^{(q\Omega)}|r_s|^2}{|r_s|^2}+2[\tan\Phi-\cos\Psi]\delta^{(q\Omega)}\tan\Phi\\&+2[\tan\Phi\sin\Psi]\delta^{(q\Omega)}\Psi_{ps}\Big\}.\end{aligned} \tag{4}$$

In Eq. (4), $\delta^{(q\Omega)}\Psi_{ps}$ is the component at $q\Omega$ of the differential of the phase difference between *s* and *p* components and is related to the bulk anisotropic modulation of the ordinary (n_o) and extraordinary (n_e) refractive indices of the polymer, known as the Kerr effect; similarly $\delta^{(q\Omega)}\tan\Phi$ is linked to the bulk anisotropic modulation of the absorption coefficient and

$$\frac{\delta^{(q\Omega)}|r_s|^2}{|r_s|^2}$$

accounts for any possible change of the whole structure reflectivity due to Kerr modulation of the polymer refractive indices.[7] The $\delta^{(q\Omega)}\Psi_{ps}$ and $\delta^{(q\Omega)}\tan\Phi$ can be obtained considering the derivatives of n_o and n_e with respect to $E(z,t)$ and then integrating all over the sample thickness. Taking into account bulk effects only, and neglecting interference effects, due to multiple reflections at the glass/ITO, ITO/polymer, and polymer/Al interfaces, one obtains, under a low birefringence approximation:[12]

$$\delta^{(q\Omega)}\Psi_{ps}=2\Lambda(\alpha)\,\mathrm{Re}[\chi^{(3)}_{zzzz}]\Gamma_q^{(q\Omega)}, \tag{5}$$

$$\delta^{(q\Omega)}\tan\Phi=2\Lambda(\alpha)\,\mathrm{Im}[\chi^{(3)}_{zzzz}]\Gamma_q^{(q\Omega)}, \tag{6}$$

where $\Lambda(\alpha)$ is an angle-dependent prefactor:

$$\Lambda(\alpha)=\frac{2k_0}{n^2}\frac{\sin^2\alpha}{\sqrt{n^2-\sin^2\alpha}}, \tag{7}$$

where k_0 is the vacuum wave vector and n is the average linear refractive index.

Equations (5) and (6) were obtained assuming complete disorder of the polymer film, so that the second-order nonlinear susceptibility $\chi^{(2)}$ is identically zero and $\chi^{(3)}_{zzzz}=3\chi^{(3)}_{xxzz}$,[13] and the absence of dispersion of $\chi^{(3)}$ between Ω and 2Ω.

Experimentally, the measurements are performed detecting the ac signal in the two bias points Ψ_c^A and Ψ_c^B defined by $\Psi_c^{A,B}+\Psi_{ps}=\pm\pi/2$. The following quantities may then be evaluated:

$$\begin{aligned}\Delta^{(q\Omega)}&=\frac{P_{\rm ac}^{(q\Omega)}(\Psi^A)-P_{\rm ac}^{(q\Omega)}(\Psi^B)}{2P_{\rm dc}(\Psi^{A,B})}=\frac{2\tan\Phi}{1+(\tan\Phi)^2}\delta^{(q\Omega)}\Psi_{ps}\\&\cong\delta^{(q\Omega)}\Psi_{ps},\end{aligned} \tag{8}$$

$$\Sigma^{(q\Omega)}=\frac{P_{\mathrm{ac}}^{(q\Omega)}(\Psi^A)+P_{\mathrm{ac}}^{(q\Omega)}(\Psi^B)}{2P_{\mathrm{dc}}(\Psi^{A,B})}=\frac{2\tan\Phi}{1+(\tan\Phi)^2}\delta^{(q\Omega)}\tan\Phi + \frac{\delta^{(q\Omega)}|r_s|^2}{|r_s|^2}\cong\delta^{(q\Omega)}\tan\Phi+\frac{\delta^{(q\Omega)}|r_s|^2}{|r_s|^2}, \tag{9}$$

where the approximations are valid for $\tan\Phi\cong 1$, valid in our experimental conditions.[14]

In EA, the light beam is not polarized and can be represented by the superposition of two mutually incoherent beams of equal amplitude, polarized in two directions orthogonal each to the other and to the propagation direction. In this way it is still possible to consider two independent waves s and p, transporting half of the total power for each. Formula (3) can be adapted to EA by deleting the interference term due to the presence of the two polarizers:

$$P_{\mathrm{dc}}\equiv P_0 R=\tfrac{1}{2}P_0|r_s|^2[1+(\tan\Phi)^2], \tag{10}$$

where the mean reflectivity of the structure $R=(|r_s|^2+|r_p|^2)/2$ is the parameter usually considered in literature in the EA measurements. Differentiating Eq. (10) leads to the expression for the modulated power:

$$P_{\mathrm{ac}}^{(q\Omega)}=\delta^{(q\Omega)}P_{\mathrm{dc}}=P_0\delta^{(q\Omega)}R=\frac{1}{2}P_0|r_s|^2\left\{[1+(\tan\Phi)^2]\frac{\delta^{(q\Omega)}|r_s|^2}{|r_s|^2}+2\tan\Phi\,\delta^{(q\Omega)}\tan\Phi\right\}. \tag{11}$$

At this point, it should be noted that the normalized reflectance variation measured in EA,

$$\frac{\delta^{(q\Omega)}R}{R}=\frac{\delta^{(q\Omega)}|r_s|^2}{|r_s|^2}+\frac{2\tan\Phi}{1+(\tan\Phi)^2}\delta^{(q\Omega)}\tan\Phi=\Sigma^{(q\Omega)} \tag{12}$$

corresponds exactly to the normalized $\Sigma^{(q\Omega)}$ signal of the EO.

Both in EO and EA the signals at frequency Ω and 2Ω are proportional to $\Gamma_1^{(\Omega)}$ and $\Gamma_2^{(2\Omega)}$, respectively. Such integrals must be evaluated with care, as already shown elsewhere.[7] Here, we shall extend the analytical model previously introduced[7] to account for the new experimental features observed. Resuming the main considerations we can say that:

(1) A charge distribution can be created inside the OXA1-PPV film. This charge is altered by an external static voltage applied for a certain time and contributes to determine the total internal electric field profile.
(2) The insulator model is not satisfying. Large offsets of the zero signal condition are observed in the measurements with both techniques and suggest some mechanism modifying the shape of $E_s(z)$ and $E_m(z)$.
(3) The signal $\Delta^{(\Omega)}$ comes from the bulk of the polymer. $\Sigma^{(\Omega)}$ comes from the bulk in the case of the EA ($\Sigma=-\Delta R/R$) and mainly from an interface contribution in the case of EO, depending on the particular wavelength range used in each experiment.
(4) The probe light interacts with the charge distribution in the case of the EA, activating the detrapping/ejection of charge carriers.

In the model, screening of the electric field is taken into account by using the Debye–Hückel approach, with a uniform screening length λ. Such approach is consistent with a model for the polymer material in which the low macroscopic mobility of carriers is due to the hopping mechanism from a conjugation segment to the other, requiring a certain activation energy, whereas the movement of the charge along a conjugation length is fast enough to follow the field at frequency Ω, resulting in a screening of the electric field.

The charge profile $\rho(z,t;V_{\mathrm{bias}})$ induced by the application of a bias voltage V_{bias}, depends on the position z inside the polymer layer ($z=0$ ITO, $z=h$ Al) and, in our previous work, was modeled, in a first-order approximation, with a step-like distribution of positive carriers located close to the ITO electrode. Here we extend this model to the case in which positive charges are uniformly distributed in the polymer film except two depletion regions close to the injecting electrodes, with different widths. This according to the fact that the previously computed electric field[7] close to the polymer/ITO interface is of the order of 10^9 V/m and can be sufficiently large to eject carriers from the very first layer of the polymer film. Then $\rho(z,t;V_{\mathrm{bias}})$ is modeled by a three parameter step-like function defined as:

$$\begin{aligned}\rho&=0, \quad 0\leqslant z\leqslant d_1,\\ \rho&=\rho_0, \quad d_1\leqslant z\leqslant d_2,\\ \rho&=0, \quad d_2\leqslant z\leqslant h,\end{aligned} \tag{13}$$

where ρ_0, d_1, and d_2 depend slowly on t for a given V_{bias}.

Under these hypotheses the potential and electric field dependencies in the film and the integrals $\Gamma_1^{(\Omega)}$ and $\Gamma_2^{(2\Omega)}$ can be easily calculated,[15] when taking into account screening with a screening length λ. We obtain

$$\Gamma_1^{(\Omega)}=\frac{\gamma_1 V_m}{4\lambda}\left\{\gamma_1\gamma_3(V_s+V_{\mathrm{bi}})+\frac{\lambda^2\rho_0}{\varepsilon}\left[-\frac{\gamma_2\gamma_3}{2}+\gamma_4-\gamma_5\right]\right\} =\kappa\frac{V_m}{h}(V_s+V_{\mathrm{bi}}+V_{\mathrm{DH}}), \tag{14}$$

$$\Gamma_2^{(\Omega)}=\frac{\gamma_1^2\gamma_3 V_m^2}{4\lambda}=\kappa\frac{V_m^2}{h}, \tag{15}$$

where

$$\gamma_3\equiv 1-e^{-2h/\lambda}+2\frac{h}{\lambda}e^{-h/\lambda}, \tag{16}$$

$$\gamma_4 \equiv -\frac{d_1}{\lambda}e^{-d_1/\lambda} - \frac{1}{2}e^{-(h-d_1)/\lambda} + \frac{1}{2}e^{-(h+d_1)/\lambda} - \frac{h-d_1}{\lambda}e^{-(h-d_1)/\lambda} - \frac{1}{2}e^{-(d_1/\lambda)} + \frac{1}{2}e^{-(2h-d_1)/\lambda}, \tag{17}$$

$$\gamma_5 \equiv -\frac{d_2}{\lambda}e^{-d_2/\lambda} - \frac{1}{2}e^{-(h-d_2)/\lambda} + \frac{1}{2}e^{-(h+d_2)/\lambda} - \frac{h-d_2}{\lambda}e^{-(h-d_2)/\lambda)} - \frac{1}{2}e^{-(d_2/\lambda)} + \frac{1}{2}e^{-(2h-d_2)/\lambda}, \tag{18}$$

$$\kappa \equiv \frac{\gamma_1^2\gamma_3}{4}\frac{h}{\lambda}, \tag{19}$$

$$V_{\mathrm{DH}} = \frac{\lambda^2\rho_0}{\varepsilon}\left(-\frac{\gamma_2}{2\gamma_1} + \frac{\gamma_4-\gamma_5}{\gamma_1\gamma_3}\right). \tag{20}$$

We remark that, due to the fact that the $\rho(z,t;V_{\mathrm{bias}})$ is time and bias dependent, $\Gamma_1^{(\Omega)}$ is slowly dependent on time and bias too and that the V_s voltage that is necessary to apply to make it zero depends on the additional term V_{DH}, that is related in a complicated manner material's parameters. In particular V_{DH} is identically zero if there is no screening ($\lambda=\infty$). In this case the modulating field $E_m(z)$ will be uniform across the film thickness, depending exclusively on V_m and not on the charge density ρ, and the $\Gamma_1^{(\Omega)}$ factor can be more simply evaluated carrying out E_m from the integral of Eq. (1):

$$\Gamma_1^{(\Omega)} = \int_0^h E_s(z)E_m dx = \frac{V_m}{h}\int_0^h E_s(z)dx = (V_s+V_{\mathrm{bi}})\frac{V_m}{h}. \tag{21}$$

Under such conditions the EO and EA signals would be zero for $V_s=-V_{\mathrm{bi}}$, where the built-in voltage drop V_{bi} is due to the difference between the two electrodes' work functions.

Even in the presence of screening, the $\Gamma_1^{(\Omega)}$ factor can get zero, for a uniform $\rho(z)$ distribution across the film thickness or for a $\rho(z)$ symmetrical respect to the $z=h/2$ position. In general, if the total positive charge present in one half of the film thickness near the ITO anode is larger than that in the half near the Al cathode, then V_{DH} is negative, otherwise V_{DH} is positive.

IV. EXPERIMENTAL RESULTS

We measured the EO and EA signals when changing either the V_s or the V_m voltage amplitudes in order to characterize charge injection at the electrode–polymer interfaces. In the following we report the results of the measurements for each of the two techniques.

Measurements of the signal P_{ac} versus the static voltage V_s, for a fixed V_m and frequency Ω, show a complex and not always repeatable behavior. Some preliminary considerations can be done starting from a time-dependent EO measurement of the signal for a sample undergoing a switch of the static voltage V_s from $+7$ to -7 V, shown in Fig. 1. It is possible to observe a long transient that lasts more than 10 min. Similar features, common to EA transient measurements, are due to the same carriers injection/ejection phenomena responsible of hysteresys cycles in I/V measurements. With such a premise, it is correct to expect from the measurements at Ω vs V_s a result that is dependent on the speed of the measurement itself. The two most relevant cases are: measurement of the signal after the complete exhaustion of the transient, and measurement of the signal immediately after an abrupt change of V_s.

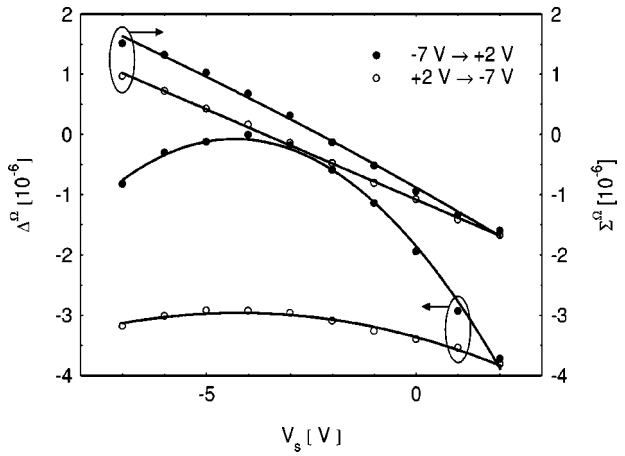

FIG. 2. EO static measurements of $\Delta^{(\Omega)}$ and $\Sigma^{(\Omega)}$, calculated with Eqs. (8) and (9) at Ω, when V_s is scanned from -7 to $+2$ V and then back from $+2$ to -7 V, for fixed $V_m=3$ V, $\Omega/2\pi=1680$ Hz, $\alpha=45°$. The solid lines are guides for the eye.

A. EO measurements as a function of V_s

We report in Fig. 2 the measurement for $\Sigma^{(\Omega)}$ and $\Delta^{(\Omega)}$ obtained when V_s is scanned from -7 to $+2$ V and then back from $+2$ to -7 V, with a step of 1 V, while the other parameters are set as follows: $\Omega/2\pi=1680$ Hz, $V_m=3$ V, $\alpha=45°$. The measurements were performed by changing V_s and then keeping it fixed for 15 min so as to wait for complete exhaustion of the transient shown in Fig. 1. At the end of the waiting time the signal is measured in both the bias points before switching V_s to the subsequent value. In this way the signals in the two bias points refer to the same space charge distribution, depending on V_s, allowing one to evaluate $\Sigma^{(\Omega)}$ and $\Delta^{(\Omega)}$.

It is possible to make two main considerations from data reported in Fig. 2. First, the $\Delta^{(\Omega)}$ signal, attributable to the bulk electro-optic effect, is absolutely not linear on V_s. The two branches of the measurement result in a strong hysteresis, indicating that the waiting time used (15 min) is not sufficient for the charge profile $\rho(z,t;V_s)$ to reach a stationary condition $\rho(z,\infty;V_s)$. Second, the $\Sigma^{(\Omega)}$ signal is approximately linear on V_s. The smaller offset between the two branches of the cycle indicate that this signal is less sensitive to the dynamics of charge redistribution inside the active layer, as if arising mainly from some interface effect contributing to the reflectivity term $\delta|r_s|^2/|r_s|^2$.

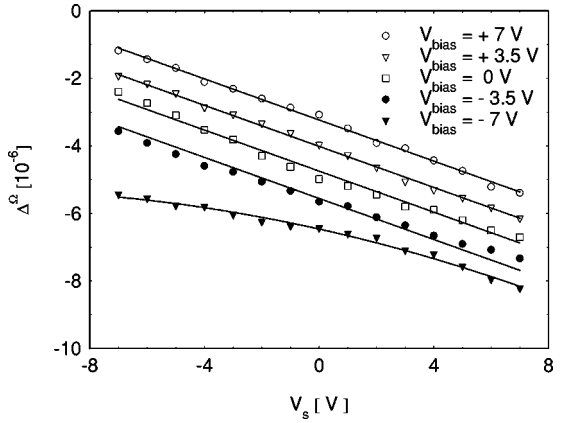

FIG. 3. Flash measurements of $\Delta^{(\Omega)}$, calculated with Eq. (8), vs V_s at $V_m=3$ V, $\Omega/2\pi=1680$ Hz, $\alpha=45°$. The solid lines are guides for the eye.

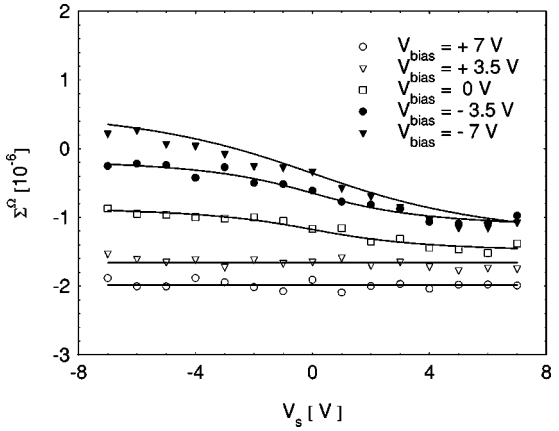

FIG. 4. Flash measurements of $\Sigma^{(\Omega)}$, calculated with Eq. (9), vs V_s at $V_m=3$ V, $\Omega/2\pi=1680$ Hz, $\alpha=45°$. The solid lines are guides for the eye.

Measurements can be carried out in a different way that allows one to better probe the effective charge distribution in the polymer layer.[7] The sample is initially biased to a fixed voltage V_{bias} for a prolonged time $\Delta t_{\text{in}}=1$ h, in correspondence of which it reaches a stationary charge distribution $\rho(z,\infty;V_{\text{bias}})$. The offset voltage is then switched to a measurement value V_s for a very short time interval during which the signal is measured; after that the voltage is returned to V_{bias} and it is kept at such value for Δt_{bias} before switching again to the subsequent V_s. The aim is to measure the signal response to the static external voltage V_s, and its associated electric field, while keeping the charge distribution frozen to $\rho(z,\infty;V_{\text{bias}})$. During the measurement V_s is scanned from -7 to $+7$ V and then back from $+7$ to -7 V, with a step of 1 V and with a $\Delta t_{\text{bias}}=20$ s, repeating and averaging five times for both points and for each valueof V_s while the other parameters have been set at $\Omega/2\pi=1680$ Hz, $V_m=3$ V, $\alpha=45°$.

In Fig. 3 we report the measurements for $\Delta^{(\Omega)}$ obtained with such method for five different values of V_{bias}. Differently from measurements shown in Fig. 2, the dependence on V_s is linear. The common slope of the curves depends on the intensity of the bulk electro-optic response, while the mutual offset depends on the charge profile inside the active layer. According to the model of Eq. (22), the offset voltage necessary to null the signal should be equal to $V_{\text{bi}}=0.4$ V, while it may reach values less than -20 V for negative V_{bias}. The most striking result is not the absolute value of this offset, but its sign, being opposite to that obtained for the thicker samples studied previously.[7]

In Fig. 4 it is reported the calculated $\Sigma^{(\Omega)}$ parameter corresponding to the same measurements of Fig. 3. The curves are substantially horizontal and independent of V_s. This behavior is consistent with our interpretation, in which we ascribe most of the observed $\Sigma^{(\Omega)}$ signal to the $(\delta^{q\Omega}|r_s|^2)/|r_s|^2$ term, related to a modulation of the polymer (average) refractive index close to the polymer/ITO interface due to the filling/emptying of surface states, and independent from the electric field in the bulk of the polymer. In this sense, to different V_{bias} correspond different levels of surface states filling. Further, the curves deviate from horizontality for the V_{bias} and in the V_s range for which $\Delta^{(\Omega)}$ deviates from linearity and from the common slope (i.e., when a space charge redistribution is supposed to take place during the measurement time, involving interfacial layer too).

Measurements of the signal P_{ac} at frequency Ω versus the modulating voltage V_m follow the linear dependence of Eq. (14). At the same time, the parameters at 2Ω are independent of V_s and quadratic on V_m, as predicted by Eq. (15); these measurements however are not reported here.

B. EA measurements as a function of wavelength

Measurements of the signal $-\delta R/R$ versus the wavelength λ of the light beam were performed both at Ω and 2Ω. The electroabsorption spectra at Ω, reported in Fig. 5, were measured for different values of the static voltage V_s, while the other parameters were set as follows: $\Omega/2\pi=1920$ Hz, $V_m=6\sqrt{2}$ V, $\alpha=45°$. The curves are similar, with a primary peak that occurs for $\lambda=490$ nm, while it is evident that the intensity of the signal is proportional to V_s. This agrees with the relationship of Eq. (21), though the dependence on V_s is clearly not linear and the difference between the two extremal curves cannot be due exclusively to the built in potential $V_{\text{bi}}=-0.4$ eV, and charge redistribution has to be

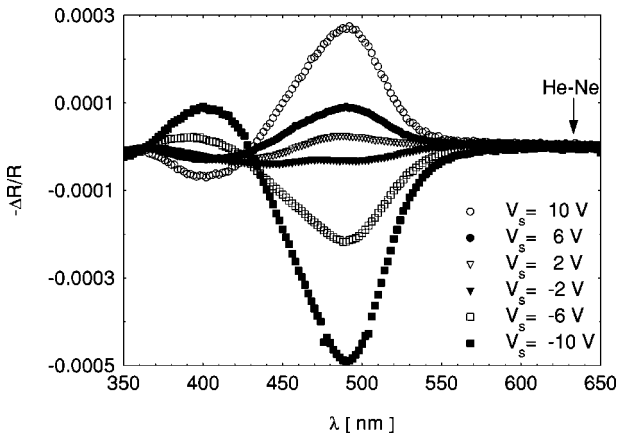

FIG. 5. EA spectra obtained for different values of V_s.

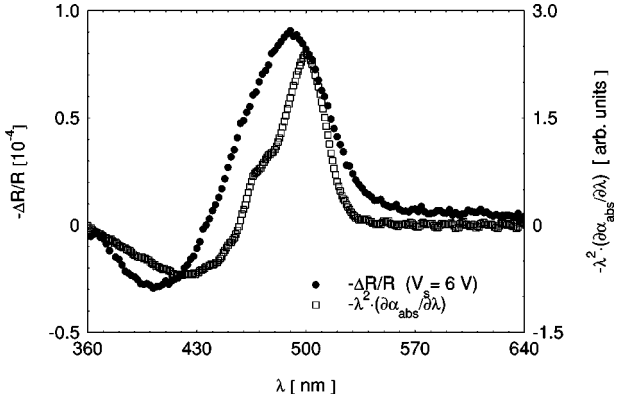

FIG. 6. EA spectrum obtained for $V_s = 6$ V compared to a function of the linear absorption coefficient.

considered. From Fig. 5 it can be noticed that at the wavelength of the He–Ne laser used in the EO setup ($\lambda_0 = 632.8$ nm) the signal is too weak to be appreciated with the EA setup, being far away from the optical resonance region.

Comparison of the measured EA spectra with the $-\lambda^2(\partial\alpha_{\mathrm{abs}}/\partial\lambda$ function, obtained from the measurement of the linear absorption spectrum of OXA1-PPV in solution, is reported in Fig. 6, and shows that electroabsorption spectra in the low energy region can be interpreted exclusively in term of neutral excitations, analogous to what is reported in the literature for other PPV derivated polymers.[16] To our extent this confirms that the electroabsorption signal derives from the bulk of the active layer, through a modulation of the absorption coefficient.

Spectral measurements at 2Ω are not reported here since they are similar to the Ω ones and, as expected from Eq. (16), do not depend on the static voltage V_s.

C. EA measurements as a function of V_s

Measurements of the signal $-\delta R/R$ versus the static voltage V_s were performed at the peak's wavelength of the electroabsorption spectra, $\lambda_0 = 490$ nm. In Fig. 7 V_s is scanned from -10 to $+10$ V and then back to -10 V with a step of 1 V, while the other parameters are set as in the previous

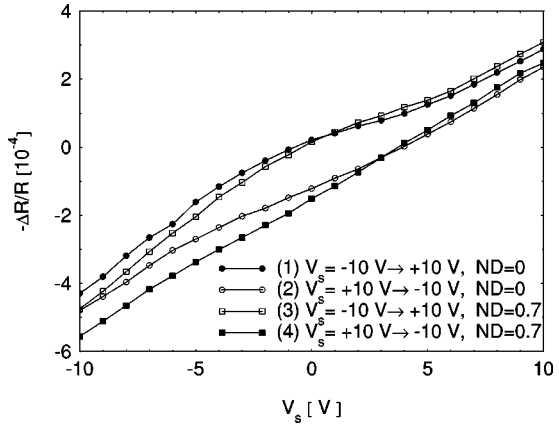

FIG. 7. EA signal vs V_s obtained for different intensities of the probe beam.

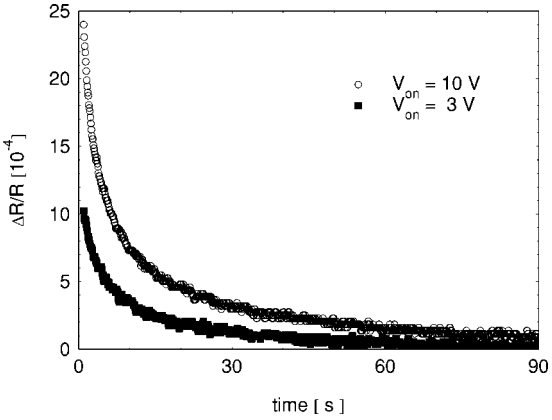

FIG. 8. EA transient measurements obtained for different values of V_{on}.

measurements: $\Omega/2\pi = 1920$ Hz, $V_m = 6\sqrt{2}$ V, $\alpha = 45°$. It can be noticed that the signal is not linear on V_s, and a marked hysteresis is present. Similar curves have been observed previously with the same experimental technique on other organic polymer samples.[8] The V_s cycles were measured for different intensities I_0 of the probe light beam, obtained by means of a neutral density filter (ND = 0.7), showing a dependence of the hysteresis amplitude on the impinging light power. This, together with the fact that the offset is notably smaller with respect to the analogue electro-optic measurements, makes it interesting to investigate further the dependence of the signal on the intensity and the wavelength of the light beam.

The deviation from the linear behavior predicted by the simplified insulator model [Eq. (21)], can be ascribed to an additional internal electric field due to the charge trapped inside the polymer film, and the hysteresis to the different dynamics in the injection/ejection of the charge carriers.

D. EA transient measurements for different V_{on} and V_{off}

Transient measurements represent a tool to investigate the dynamics of charge redistribution. They are performed by keeping the sample under a static voltage $V_s = V_{\mathrm{on}} > 0$ V for a definite time interval t_{on}, and then switching V_s to a $V_{\mathrm{off}} \leqslant 0$ V and starting to measure the EA signal during a time interval t_{off}. The general behavior is that of a double exponential decay of the signal, due to the ejection of the charge from the active layer.

In Fig. 8 we report two transient measurements obtained for different values of V_{on}, when the other parameters are set as follows: $\lambda = 490$ nm, $\Omega/2\pi = 1920$ Hz, $V_m^{\mathrm{eff}} = 6$ V, $\alpha = 45°$, $V_{\mathrm{off}} = 0$ V, $t_{\mathrm{on}} = 40$ s, $t_{\mathrm{off}} = 90$ s. It is clear that for each curve the signal starts decaying from a different value corresponding to the respective value of V_{on} (i.e. to a different charge profile), while after the time interval t_{off} relaxes to zero.

In Fig. 9 it is reported a second series of transient measurements obtained by switching V_{on} from $+7$ V to different values of V_{off}, while the other parameters are set identically to the previous series. In this case the signals start decaying

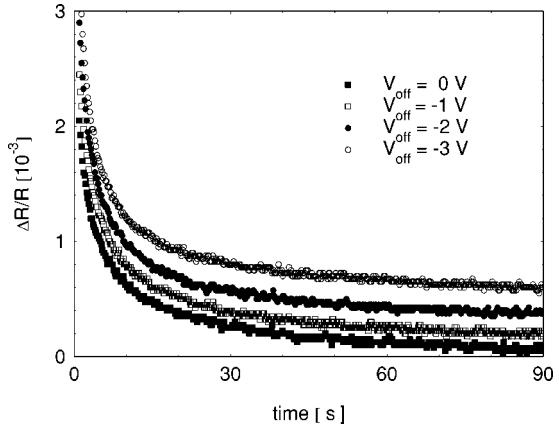

FIG. 9. EA transient measurements obtained for different values of V_{off}.

from the same point for all the curves and relax to constant values, each corresponding to a different V_{off}.

E. EA transient measurements for different probe intensities and in the presence of a pump beam

A third series of transient measurements was obtained for different intensities of the light beam, by means of neutral density filters placed at the exit of the monochromator. V_s is switched from $V_{\mathrm{on}}=+7$ V to $V_{\mathrm{off}}=0$ V, while the others parameters are set as in the previous series. Figure 10 shows that in the curves corresponding to a lower probe beam intensity the signal decays to upper levels, indicating a slower dynamics of internal electric field redistribution and a residue of trapped charge in the polymer film. Such a behavior suggests that the measurement light beam activates the detrapping and ejection of charge carriers (i.e., holes).

To further investigate this mechanism, a *pump–probe* series of transient measurements has been performed. To this aim the electroabsorption setup has been modified introducing a second lamp and a monochromator, and a neutral density filter (ND=1) on the path of the probe beam to ensure that its effects would be negligible with respect to those due to the pump beam. The other parameters are set in the following way: $\lambda_0=486$ nm, $\Omega/2\pi=1920$ Hz, $V_m^{\mathrm{eff}}=3.5$ V,

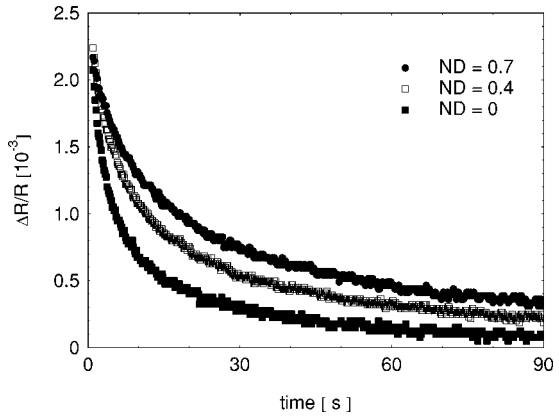

FIG. 10. EA transient measurements obtained for different intensities of the probe beam.

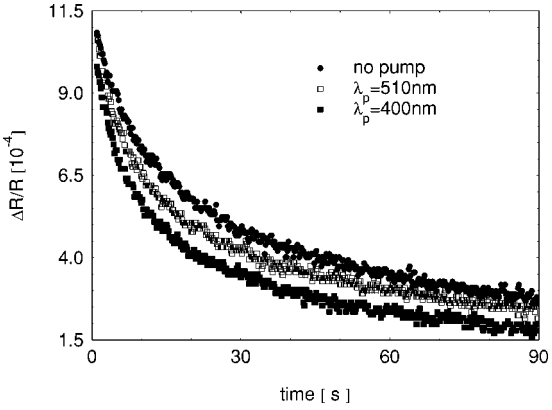

FIG. 11. Transient measurement signal vs V_s obtained for two different wavelengths of the pump beam compared with the transient in the absence of the pump.

$\alpha=45°$, $V_{\mathrm{on}}=+7$ V, $V_{\mathrm{off}}=0$ V, $t_{\mathrm{on}}=50$ s, $t_{\mathrm{off}}=90$ s. Measurements for seven different values of the pump beam wavelength λ_p varying from 550 and 400 nm were performed, plus two control measurements in the absence of pump at the beginning and at the end of the series. In Fig. 11 we report the three most significant pump–probe measurements, the others being intermediate or overlapping to these curves. It can be noticed that the presence of the pump has an effect similar to that of changing the intensity of the probe beam, accelerating the detrapping/ejection of charge carriers. This effect is enhanced when λ_p crosses the maximum electroabsorption response ($\lambda_0=490$ nm). The initial and the final curves obtained in the absence of the pump overlap, indicating that the sample was not damaged during the execution of the pump–probe transient series.

V. DISCUSSION

In this section, we shall first analyze the EO data using the model introduced to get some quantitative evaluations on the space-charge distribution. Then we shall analyze the EA data to further investigate the redistribution phenomena, and to obtain more information on the nature of the charge by means of a comparison between the two techniques.

As already seen, the $\Delta^{(\Omega)}$ vs V_s curves of Fig. 3 show a linear behavior indicating that the corresponding charge distributions are effectively kept fixed during the measurements. The offset voltage V_{DH} to null the signal is very large in the present case ($h=200$ nm, $V_{\mathrm{DH}}=+8$ V to $+20$ V), as in the samples previously studied ($h=285$ nm, $V_{\mathrm{DH}}=-10$ V to -20 V), but with opposite sign. According to the analytical model, it is necessary to assume that a net positive charge is resident in the second half of the active layer, near to the Al cathode.

Substituting the expressions derived with the analytical model for $\Gamma_1^{(\Omega)}$ and $\Gamma_2^{(2\Omega)}$ (14) and (15) in Eqs. (5) and (8) for the phase shift term $\delta^{(q\Omega)}\Psi_{ps}$ and for the signals $\Delta^{(q\Omega)}$, one obtains

$$\Delta^{(\Omega)}=\Lambda(\alpha)\mathrm{Re}[\chi^{(3)}_{zzzz}]\kappa\frac{V_m}{h}(V_s+V_{\mathrm{bi}}+V_{\mathrm{DH}}), \qquad (22)$$

TABLE I. Values of the prefactor in Eqs. (22) and (23) (column 3) are reported for three successive EO measurements of $\Delta^{(\Omega)}$ vs V_s, similar to those reported in Fig. 3, for different values of V_{bias}. In column 4 we report the ratio of such values to the same quantities evaluated from the fit of an independent $\Delta^{(2\Omega)}$ vs V_m measurement. In columns 5–7 estimated for the offset voltage V_{DH}, charge density, and depletion width d_1 obtained by the fits are reported.

Series	V_{bias} (V)	$\Lambda(\alpha)\text{Re}[\chi^{(3)}_{zzzz}]\kappa$ (m/V^2)	β	V_{DH} (V)	ρ_0/e (m^{-3})	d_1 (nm)
c	+3.5	2.01×10^{-14}	1.01	+9.6	0.74×10^{24}	100
c	+7	1.97×10^{-14}	0.99	+8.1	0.74×10^{24}	70
d	+3.5	2.05×10^{-14}	1.03	+14.4	1.11×10^{24}	100
d	+7	1.89×10^{-14}	0.95	+12.9	1.11×10^{24}	75
f	+3.5	2.05×10^{-14}	1.03	+13.5	1.21×10^{24}	71
f	+7	2.03×10^{-14}	1.02	+11.0	1.21×10^{24}	57

$$\Delta^{(2\Omega)}=\frac{1}{4}\Lambda(\alpha)\text{Re}[\chi^{(3)}_{zzzz}]\kappa\frac{V_m^2}{h}. \tag{23}$$

Both expressions contain the same prefactor $\Lambda(\alpha)\text{Re}[\chi^{(3)}_{zzzz}]\kappa$, which can be evaluated separately by independent measurements of the signals at Ω and 2Ω, for the same incidence angle.

In Table I we resume the results obtained from fitting three different series of measurements [a, b, and c], similar to that reported in Fig. 3 and performed one after the other. For each measurement we fitted with a straight line the curves obtained for $V_{\text{bias}}=+3.5$ V and $V_{\text{bias}}=+7$ V. In column 3 the fitted values of $\Lambda(\alpha)\text{Re}[\chi^{(3)}_{zzzz}]\kappa$ are listed. In column 4 the ratio β of such values to the corresponding factor evaluated from the fit of the $\Delta^{(2\Omega)}$ vs V_m measurement (not reported here) is listed. β is always about one, showing that the agreement is good and ensuring that the three series of measurements at Ω and the V_{DH} obtained are consistent.

From Table I it can be noticed that in each series the changes of V_{DH} induced by V_{bias} are always smaller than V_{DH} itself, suggesting the presence of a stable charge distribution, with density larger than the injected one. Since theoretically $V_{\text{DH}}\propto\rho_0$ [Eq. (20)] and that the measured values decrease as V_{bias} gets larger, the injected charge is more likely reducing d_1 (i.e., filling the superficial layers) than increasing the ρ_0 in the bulk. Besides, there are larger variations of V_{DH} between different series, showing consistent charge redistribution on the long term. On this basis, Eqs. (14)–(20) can be used to estimate the spatial charge distribution, in terms of ρ_0, d_1, and d_2. We optimized the values of the parameters, setting the penetration depth equal to the thickness of the active layer ($d_2=h$), considering ρ_0 constant in each series and determining h_1 necessary to obtain the corresponding V_{DH}. The results for the charge concentration ρ_0 are consistent with data reported in literature.[17]

The charge distribution in the bulk of the polymer shows a low mobility behavior, and is probably due to carriers trapped in deep levels. However, the depletion region near the ITO electrode could still be due to the contemporary presence of OH^- ions diffused from the surface.[3] As a consequence the static electric field, negative and large, close to the ITO electrode is quite stable over time and limits the performances for PLED made out of OXA1-PPV. The nature of the stable charge distribution can be identified by analyzing the EA data.

TABLE II. Parameters obtained by fitting the EA transients with a double exponential law given by Eq. (25). The data refer to the transients executed for different values of V_{on} and V_{off} reported in Figs. 8 and 9.

V_{on} (V)	V_{off} (V)	a (10^{-4})	b_1 (10^{-4})	b_2 (10^{-4})	$a+b_1+b_2$ (10^{-4})	τ_1 (s)	τ_2 (s)
3	0	0.1	7.4	4.3	11.8	3.4	23.4
4	0	0.2	10.3	6.1	16.6	3.0	21.3
5	0	0.3	13.3	6.9	20.6	2.7	21.8
6	0	0.5	14.9	8.0	23.4	2.7	20.9
7	0	0.6	17.1	8.3	26.0	2.8	21.7
8	0	0.6	18.8	8.6	28.1	2.8	22.4
9	0	0.8	19.3	9.3	29.4	2.7	21.8
10	0	0.9	18.5	9.3	28.7	2.8	21.9
				⋯			
7	0	0.6	16.1	8.1	⋯	2.7	21.4
7	−1	2.0	18.7	8.9	⋯	2.8	20.1
7	−2	3.8	22.4	9.1	⋯	2.7	18.9
7	−3	6.1	26.3	8.7	⋯	2.5	20.8

TABLE III. Parameters from the fit of the EA transients for different intensities of the probe beam in standard relaxation measurements and of the wavelength in the pump–probe measurements. All the measurements are performed at $\lambda = 490$ nm switching V_s from $V_{on} = +7$ V to $V_{off} = 0$ V, while for the pump–probe experiment ND = 1 for the probe beam to ensure its effects would be negligible with respect to that due to the pump beam.

ND	a (10^{-4})	b_1 (10^{-4})	b_2 (10^{-4})	τ_1 (s)	τ_2 (s)
1	3.8	4.2	11.9	6.6	41.4
0.7	2.6	8.5	11.8	5.9	33.4
0.4	1.9	11.9	10.8	4.5	28.0
0.2	1.2	14.3	10.0	3.5	24.2
0	0.7	15.4	8.25	3.1	23.3
λ_p (nm)	a (10^{-4})	b_1 (10^{-4})	b_2 (10^{-4})	τ_1 (s)	τ_2 (s)
No pump	2.0	4.6	4.5	8.4	49.1
550	2.0	4.2	5.0	7.3	45.9
530	2.0	4.5	4.8	6.6	42.4
520	2.0	4.3	5.0	6.2	39.0
510	2.0	4.5	4.9	5.4	36.7
500	1.8	5.0	4.9	3.4	29.8
450	1.8	4.5	4.6	4.6	32.9
400	1.5	4.5	4.7	4.9	33.7

We wish to remark that in the EO ($\lambda = 632.8$ nm), the $\Sigma^{(q\Omega)} = \delta^{(q\Omega)} R/R$ signal is mainly due to the $(\delta^{(q\Omega)}|r_s|^2)/|r_s|^2$ term, dominated by a strong reflectivity modulation term. This is suggested by the $\Sigma^{(\Omega)}$ vs V_s measurements reported in Fig. 4, which show an independence from the static electric field in the bulk. Measurements as a function of the incidence angle α (not reported here) strengthen this interpretation.[7]

In the EA, the signal originates mainly from a modulation of the absorption coefficient in the bulk of the polymer film, as introduced in Sec. IV B. The signal due to this effect[18] is proportional to the overlap integral $\Gamma_1^{(\Omega)}$ through the constant $\mathrm{Im}[\chi^{(3)}_{zzzz}]$, which is not negligible in the absorption band and leads to a linear dependence on V_s, similar to what happens for $\Delta^{(\Omega)}$. However the static measurements of $\delta^{(\Omega)} R/R$ vs V_s show smaller hysteresis effects and offset respect to the EO analogue. Further, the EA transients induced by a step of V_s are faster than the corresponding EO dynamic measurements. As a conclusion, the charge distributions observed with the two techniques must be different.

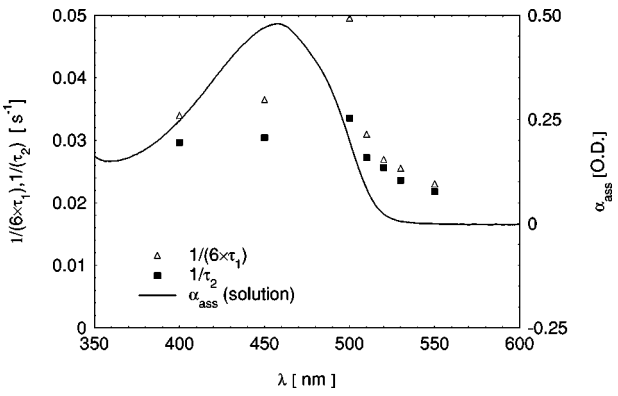

FIG. 12. Time constants of the pump–probe EA transients expressed as decay rates vs the wavelength of the pump and absorption spectrum of OXA1-PPV in solution.

To further investigate such differences, we fitted the EA transients with a double exponential function:

$$\frac{\delta R}{R}(t) = a + b_1 \exp\left(-\frac{t}{\tau_1}\right) + b_2 \exp\left(-\frac{t}{\tau_2}\right), \qquad (24)$$

which describes the temporal dependence better than a single exponential. In Table II we report the parameters of the fits for the first two series of transients, executed, respectively, at different values of the V_{on} and of the V_{off}, reported in Figs. 8 and 9. The signal $(\delta R/R)(t=0) = a + b_1 + b_2$ is proportional to V_{on} and saturates at high voltage. Besides, the value to which the signal decays $(\delta R/R)(t=\infty) = a$ is proportional to V_{off}. This is consistent with the fact that after the negative step in V_s the charge is totally ejected and the signal keeps proportional to the internal static electric field. Moreover, the time constants are nearly identical for all the measurements of the two series, and notably smaller than the analogue EO ones.

The differences in the behavior of the EO and EA measurements lead us to conclude that at least one of the two techniques influences sensibly the spatial charge. The smaller offset and the faster dynamic observed with EA can be explained attributing the stable charge to carriers trapped in deep levels that are reactivated by the absorption of the light beam. To support these indications we report in Table III the fit parameters of the EA transients obtained for different probe intensities (Fig. 10) and of the pump–probe transients (Fig. 11). It is clearly seen that at higher pump beam intensity the time constants decrease, indicating that the probe beam itself accelerates the decay. On the other side we observe a dependence of the relaxation time constants on the wavelength of the pump beam. Such behavior is better evi-

denced in Fig. 12, if we plot the values of τ_1 and τ_2 reported in Table III as a function of the wavelength of the pump beam and if we compare such data with the absorbance of a solution of OXA1-PPV.

VI. CONCLUSIONS

We reported here the comparative interpretation of electro-optic and electroabsorption measurements on oxadiazole based PPV electroluminescent films. As a main conclusion, the larger offset and slower dynamics observed with the EO setup operating outside the absorption band, with respect to the EA results, indicate that the latter nonlinear technique alters the space-charge distribution inside the active layer, by means of optical reactivation of trapped or low mobility carriers. The presence of Debye–Hückel screening is taken into account together with a new feature of the charge distribution, consisting in superficial depleted regions near the ITO and Al electrodes, generated by the strong field associated with the inner charge distribution.

ACKNOWLEDGMENTS

The authors gratefully acknowledge Z. Bao for providing the OXA1-PPV samples and M. Bertolotti, S. Paoloni, A. Belardini, and M. C. Larciprete for useful discussions. The research has been partially supported by the Italian Institute of Physics of the Matter (INFM) and European Community (Contract No. IST-2000-28018).

[1] J. Kalinowski, J. Phys. D **32**, 179 (1999).
[2] I. D. Parker, Y. Cao, and C. Y. Yang, J. Appl. Phys. **85**, 2441 (1999).
[3] J. Shen, D. Wang, E. Langlois, W. A. Barrow, P. J. Green, C. W. Tang, and J. Shi, Synth. Met. **111–112**, 237 (2000).
[4] F. Michelotti, V. Taggi, M. Bertolotti, T. Gabler, H. H. Hörhold, and A. Bräuer, J. Appl. Phys. **83**, 7886 (1998).
[5] M. Herold, W. Schmid, T. Vogtmann, R. Fischer, D. Haarer, and M. Schwoerer, Appl. Opt. **34**, 996 (1995).
[6] P. Röhl, B. Andress, and J. Nordmann, Appl. Phys. Lett. **59**, 2793 (1991).
[7] F. Michelotti, S. Bussi, L. Dominici, M. Bertolotti, and Z. Bao, J. Appl. Phys. **91**, 5521 (2002).
[8] C. Giebeler, S. A. Whitelegg, A. J. Campbell, M. Liess, S. J. Martin, P. A. Lane, D. D. C. Bradley, G. Webster, and P. L. Burn, Appl. Phys. Lett. **74**, 3714 (1999).
[9] Z. Zao, Z. Peng, M. E. Galvin, and E. A. Chandcross, Chem. Mater. **10**, 1201 (1998).
[10] J. Gao, A. J. Heeger, I. H. Campbell, and D. L. Smith, Phys. Rev. B **59**, R2482 (1999).
[11] C. Giebeler, S. A. Whitelegg, D. G. Lidzey, P. A. Lane, and D. D. C. Bradley, Appl. Phys. Lett. **75**, 2144 (1999).
[12] F. Michelotti, G. Nicolao, F. Tesi, and M. Bertolotti, Chem. Phys. **245**, 311 (1999).
[13] P. N. Butcher and D. Cotter, *The Elements of Nonlinear Optics, Cambridge Studies in Modern Optics* (Cambridge University Press, Cambridge, 1990).
[14] It is to be noted the more efficient normalization of the semi-difference and semisum signals $\Delta^{(q\Omega)}$, $\Sigma^{(q\Omega)}=[P_{\mathrm{ac}}^{(q\Omega)}(\Psi^A) \pm P_{\mathrm{ac}}^{(q\Omega)}(\Psi^B)]/2P_{\mathrm{dc}}(\Psi^{A,B})$ with respect to what was previously defined (Ref. 7), where $\Delta^{(q\Omega)},\Sigma^{(q\Omega)}=[(1+\tan\Phi)^2/8\tan\Phi\, P_{\mathrm{ac}}^{(q\Omega)}(\Psi^A)\pm P_{\mathrm{ac}}^{(q\Omega)}(\Psi^B)/P_{\mathrm{dc}}^{\max}]$.
[15] See EPAPS Document No. E-PRBMDO-69-002405 for the complete calculation. A direct link to this document may be found in the online article's HTML reference section. The document may also be reached via the EPAPS homepage (http://www.aip.org/pubservs/epaps.html) or from ftp.aip.org in the directory /epaps/. See the EPAPS homepage for more information.
[16] M. Liess, S. Jeglinski, Z. V. Vardeny, M. Ozaki, K. Yoshino, Y. Ding, and T. Barton, Phys. Rev. B **56**, 712 (1997).
[17] A. J. Campbell, D. D. C. Bradley, and D. G. Lidzey, J. Appl. Phys. **82**, 6326 (1997).
[18] We remark the different contributions to the EA signal, clearly seen when expressed as: $\delta R/R=\delta|r_s|^2/|r_s|^2+2\tan\Phi/[1+(\tan\Phi)^2]\delta\tan\Phi \cong 2/(1-R_0^s)\,\delta R_0^s - 2h\,\delta\alpha_z^s - h\,\delta(\alpha_z^p-\alpha_z^s) \cong -h\,\delta(\alpha_z^p+\alpha_z^s)$, where the term $\delta|r_s|^2/|r_s|^2$ contains a modulation of the ITO/polymer interface reflectivity index R_0 and a bulk modulation of the absorption coefficient along the z direction for the s wave, while the term $\delta\tan\Phi$ accounts for the bulk anisotropic modulation of the absorption coefficient for the two waves. The first approximation is valid if not considering the multiple reflections and for $\tan\Phi\cong 1$, moreover the difficult evaluation of $2/(1-R_0^s)\,\delta R_0^s$ can be neglected for the EA when $h\geqslant 100$ nm allowing the second approximation. See S. J. Martin, D. C. C. Bradley, P. A. Lane, H. Mellor, and P. L. Burn, Phys. Rev. B **59**, 15 133 (1999).